Supporting Information

for

Photoanodes with Fully Controllable Texture: The Enhanced Water Splitting Efficiency of Thin Hematite Films Exhibiting Solely (110) Crystal Orientation

Stepan Kment,[1,] Patrik Schmuki,[2,]* Zdenek Hubicka,[3] Libor Machala,[1] Robin Kirchgeorg,[2] Ning Liu,[2] Lei Wang,[2] Kiyoung Lee,[2] Jiri Olejnicek,[3] Martin Cada,[3] Ivan Gregora,[3] and R. Zboril[1,]**

[1] Regional Centre of Advanced Technologies and Materials, Joint Laboratory of Optics and Departments of Experimental Physics and Physical Chemistry, Faculty of Science, Palacky University, 17. listopadu 1192/12, 771 46 Olomouc, Czech Republic.

[2] Department of Materials Science and Engineering, University of Erlangen-Nuremberg, Martensstrasse 7, D-91058 Erlangen, Germany.

[3] Institute of Physics, Academy of Sciences of the Czech Republic, Na Slovance 2, 14800 Prague, Czech Republic.

* Authors to whom correspondence should be addressed: E-mail address: stepan.kment@upol.cz, schmuki@ww.uni-erlangen.de, radek.zboril@upol.cz

Number of pages: 8
Number of figures: 9
Number of tables: 1

Supporting Figures

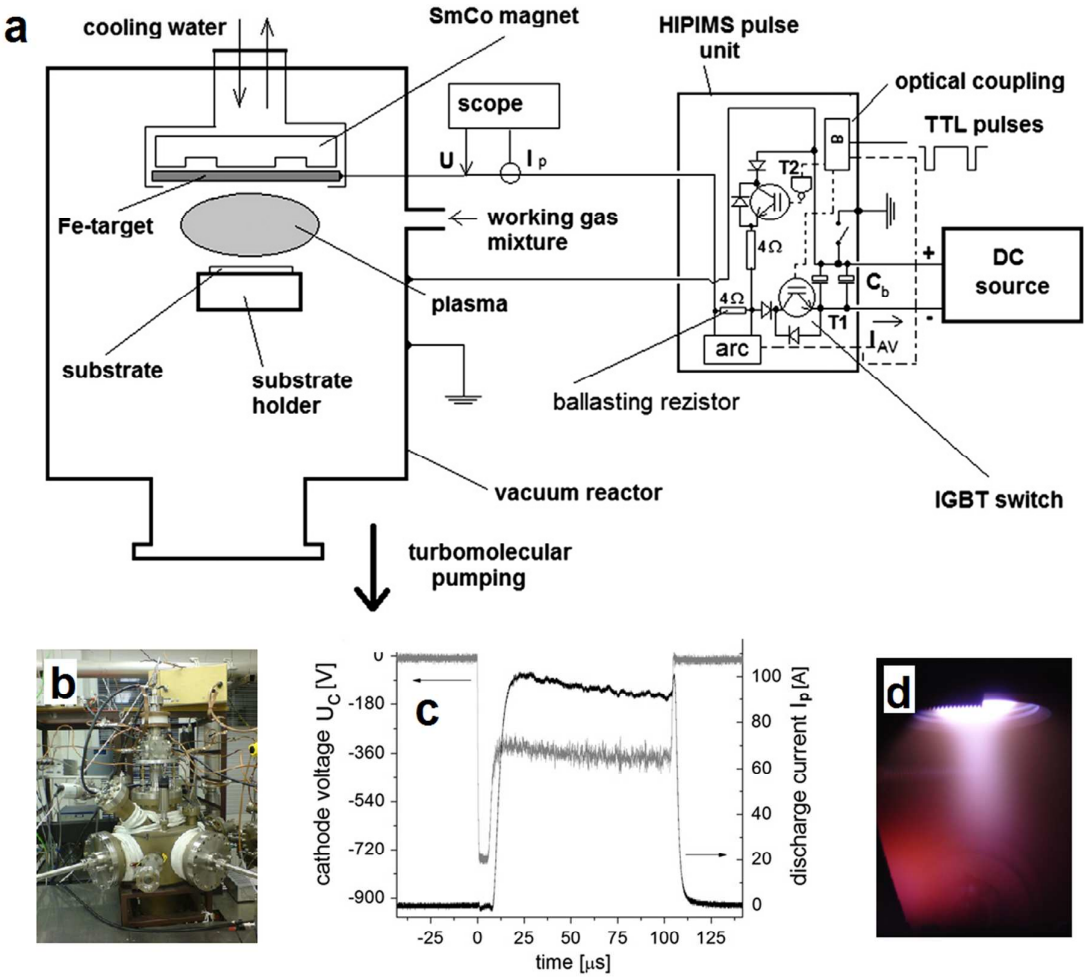

Figure S1. (a) Schematic arrangement of HiPIMS deposition system for the reactive sputtering of hematite thin films, (b) photograph of the UHV plasma-assisted deposition reactor, (c) typical discharge voltage and current waveforms obtained during reactive sputtering of Fe_2O_3 measured at the pulse HiPIMS magnetron discharge with the Fe target with applied pulse power $P_p = 34$ kW, and (d) photograph of HiPIMS plasma discharge during the deposition of the thin electrodes.

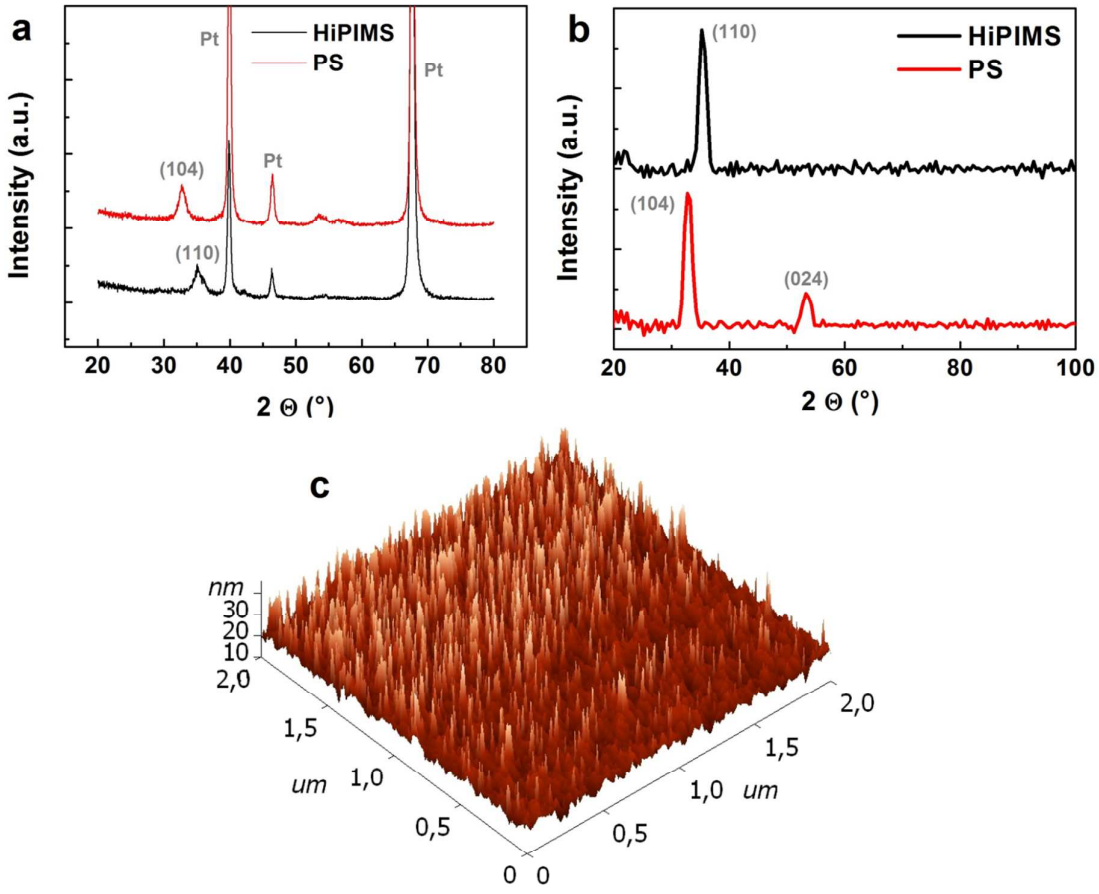

Figure S2. Extended X-ray diffraction spectra of HiPIMS and PS films deposited on the $Si/TiO_2/Pt$ substrate (a) and fused silica substrate (b). AFM 3D surface topography scan of the HiPIMS hematite film deposited on the $Si/TiO_2/Pt$ substrate.

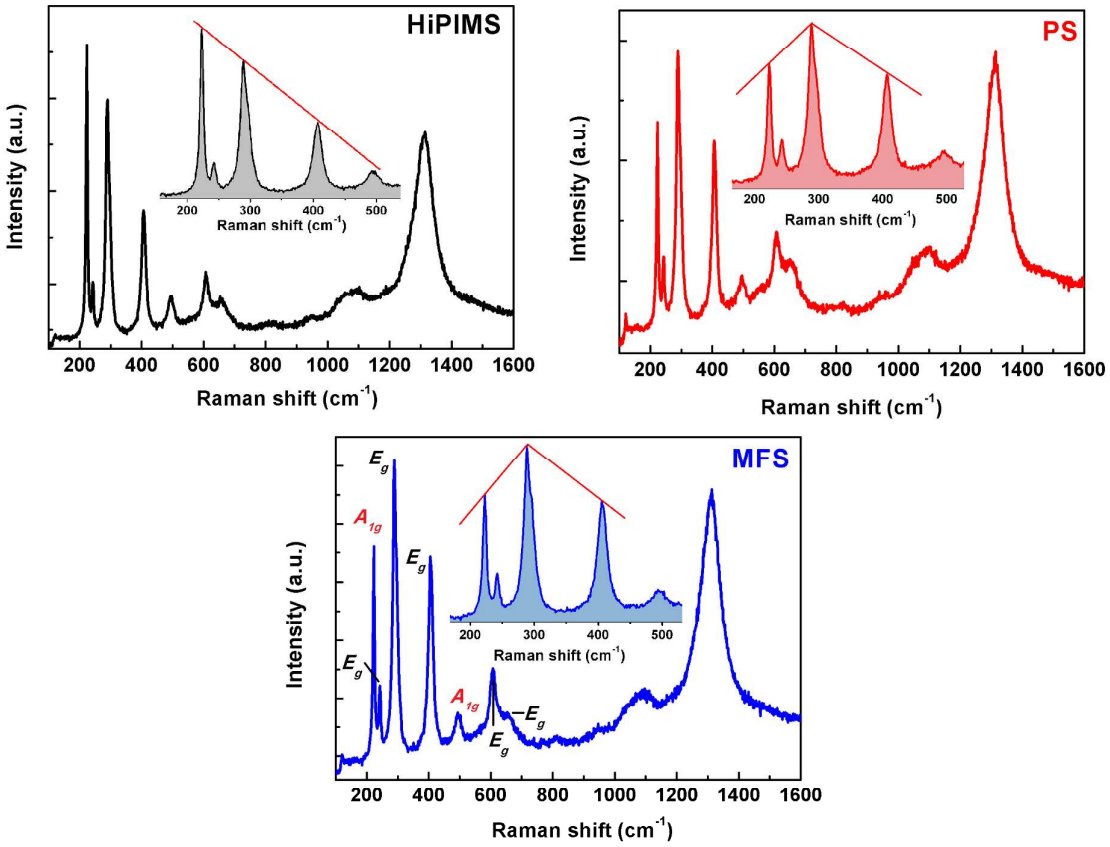

Figure S3. Raman spectra of hematite films. The Raman peak at around 1300 cm^{-1} is due to the 2-magnon scattering band.

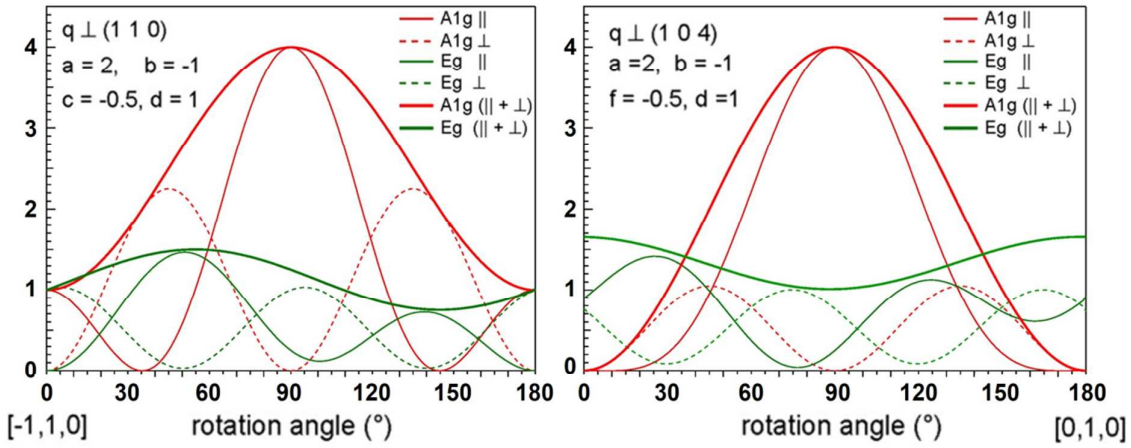

Figure S4. Modeled polarized Raman spectra as the function of sample rotation along to the normal to the surface of the HiPIMS film. Note: Under the assumption that the samples are

nanocrystalline having the same crystalline orientation perpendicular to the substrate or along its plane, it is principally possible to utilize the angle dependencies of Raman intensity, i.e., to measure polarized spectra as the function of sample rotation along to the normal to the surface. Figure S4 shows such intensity dependency of the HiPIMS film in the case of back scatterings on the planes (110) and (104) for particular choice of Raman parameters of the Raman tensors A_{1g} ($a = 2$, $b = -1$) a E_g ($c = -0.5$, $d = 1$). Solid lines correspond to the parallel polarization (||) of the incident and scattered photon and the dashed line to the cross polarization (⊥). The bold line indicates their sum, which corresponds approximately to the depolarized spectrum (only the laser is polarized and not the detector). When comparing the mean values of depolarized spectra, A_{1G} and Eg modes, one can see that the ratio of the mean scattering intensity, $I(A_{1G})/I(E_g)$, is for the surface (110) greater than for (104). Since the intensity of the lowest A_{1g} peak is considerably higher for the HiPIMS films, whereby the intensities of the E_g modes are almost identical among all the films, this simulation indicates that the preferential orientation of the HiPIMS films is along the (110) plane.

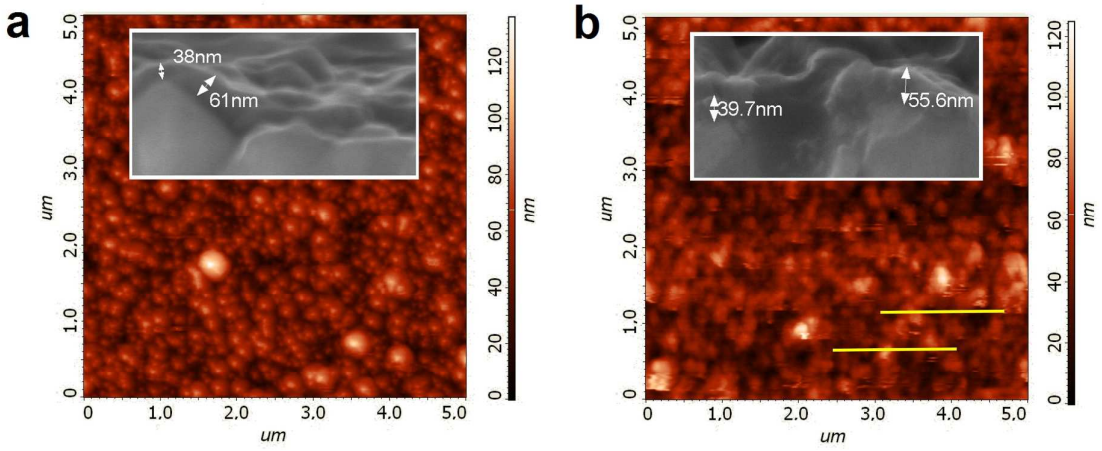

Figure S5. AFM surface topography images and SEM cross-section images of (a) MFS and (b) PS hematite films.

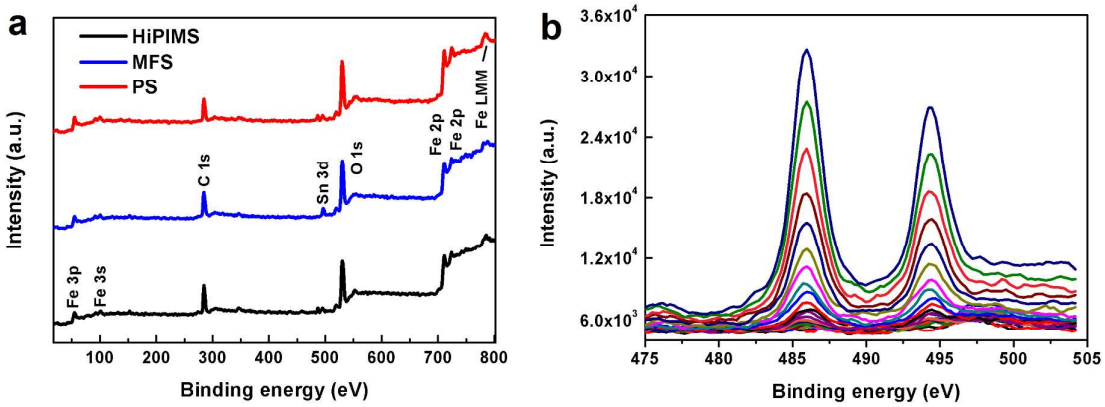

Figure S6. XPS full survey spectra of hematite films (a) and XPS high-resolution depth Sn 3d peaks' profile of the MFS film recorded after each sputtering cycle (b) – the highest intensity peaks correspond to Sn 3d signals coming from the FTO substrate and lowest intensity (no Sn 3d peaks) originated from the film.

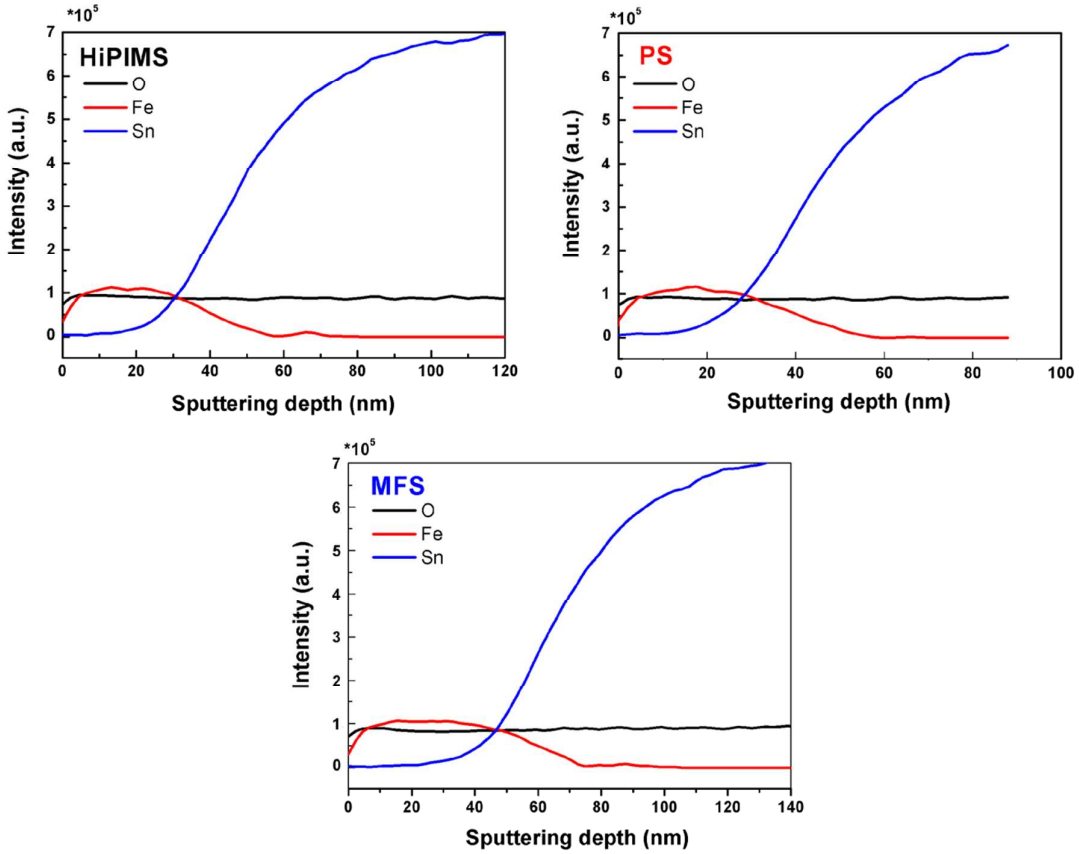

Figure S7. XPS sputtering depth profiles of O, Fe and Sn species.

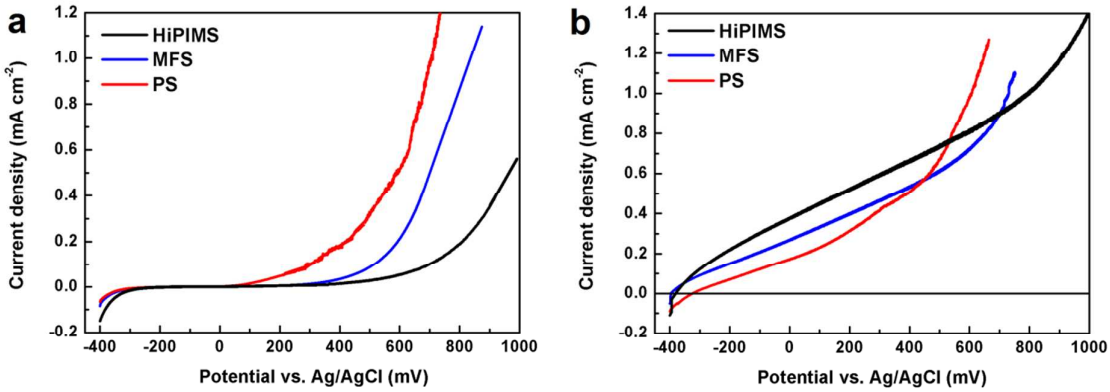

Figure S8. Current density vs. applied potential curves of the films recorded in the dark conditions (a) and under AM 1.5 illumination (100 mW cm^{-2}) in 0.5 M H_2O_2 / 1 M NaOH electrolyte as a function of applied potential with respect to the Ag/AgCl (b).

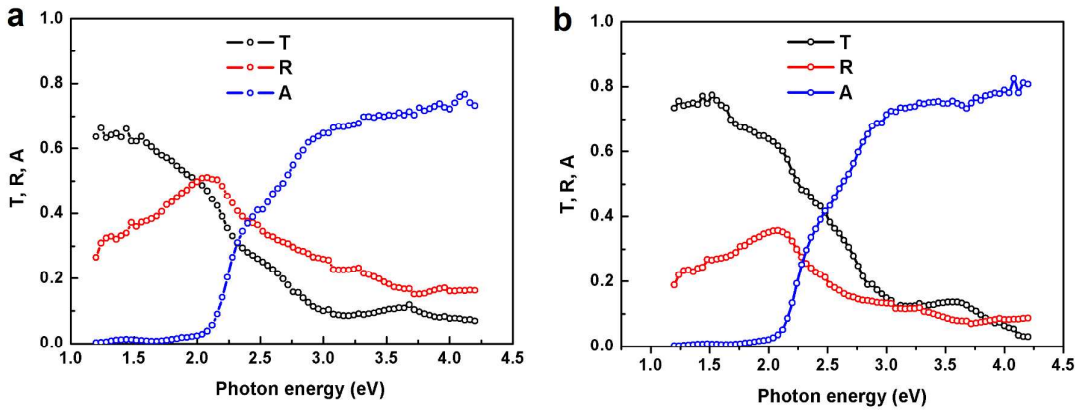

Figure S9. Optical properties of (a) HiPIMS and (b) PS fabricated photoanodes. T, R, and A denote transmittance, absorptance, and reflectance, respectively.

Supporting Table

Table S1. Hyperfine parameters and values of x and Θ of the hematite thin layers.

Sample acronym	δ_{Fe} [±0.01 mm/s]	2ε [±0.02 mm/s]	B_{hf} [±0.3 T]	x	Θ [°]
HiPIMS	0.32	–0.18	50.8	1.58 ± 0.09	48.8 ± 1.4*
PS	0.32	–0.19	50.7	2.69 ± 0.05	63.7 ± 0.6*
MFS	0.32	–0.20	51.0	2.31 ± 0.03	58.9 ± 0.4*

δ_{Fe} … isomer shift related to alpha iron at room temperature, 2ε … quadrupole shift, B_{hf} … hyperfine magnetic field, * … the errors were calculated from the errors of x.